Available online at www.sciencedirect.com
SCIENCE DIRECT®
Bioorganic & Medicinal Chemistry 13 (2005) 5819–5825
Bioorganic & Medicinal Chemistry

Amentoflavone and its derivatives as novel natural inhibitors of human Cathepsin B

Xulin Pan,[a,b] Ninghua Tan,[a,*] Guangzhi Zeng,[a,b] Yumei Zhang[a] and Ruirui Jia[a]

[a]*State Key Laboratory of Phytochemistry and Plant Resources in West China, Kunming Institute of Botany, Chinese Academy of Sciences, Kunming 650204, China*
[b]*Graduate School of the Chinese Academy of Sciences, Beijing 100039, China*

Received 14 April 2005; revised 24 May 2005; accepted 25 May 2005
Available online 3 August 2005

Abstract—Cathepsin B (CatB) is a member of the papain superfamily of cysteine proteases and has been implicated in the pathology of numerous diseases, including arthritis and cancer. Amentoflavone is found in a number of plants with medicinal properties, including *Ginkgo biloba* and *Hypericum perforatum* (St. John's Wort). Herein, we report the structure–activity relationship (SAR) and binding mechanism of three biflavones, amentoflavone (AMF1), 4‴-methylamentoflavone (AMF2) and 7″,4‴-dimethylamentoflavone (AMF3), isolated from *Taxodium mucronatum* by us as novel natural inhibitors of human CatB with strong inhibitory activities at IC_{50} values of 1.75, 1.68 and 0.55 μM, respectively. Density functional theory (DFT) method was applied to optimize the geometry structures of AMF1, AMF2 and AMF3 at the B3LYP/6-31G* level. FlexX was explored to dock the three biflavones to the binding sites of CatB, and to get a better understanding of vital interactions between these biflavones and CatB. A good correlation between the calculated quantum descriptors and the experimental inhibitory activities suggested that quantum model of these potential inhibitors is reliable. Through geometry and electron structure analysis of AMFs, it was observed that the CH_3 substitute at 7″ and 4‴ positions could not vary the difference in geometry structure significantly, but increase the electron density of A-ring, HOMO energy, hydrophobic property, and improve inhibitory activity. Structural and energetic analysis of AMFs and AMFs–CatB complexes showed that the electron-donor site is the A-ring, which shows the highest HOMO energy distribution, and the electron-acceptor site is the F-ring, which shows the highest LUMO energy distribution in AMFs, and the π–π interaction between A-ring and residue Trp221, two hydrogen bonds (O5 and Trp221; O4 and Gln23), hydrophobic interaction between the C-ring and residue Cys29 and CH_3 substitutes at 7″ and 4‴ might play a crucial role in the inhibition of AMFs on CatB. Results indicated that AMFs are new natural reversible inhibitors that would be useful in developing potent inhibitors of CatB.

1. Introduction

Human Cathepsin B (CatB, EC 3.4.22.1) is a lysosomal cysteine protease of the papain family. Its functions in intracellular protein catabolism and in certain situations may also be involved in other physiological processes, such as processing of antigens in the immune response, hormone activation and bone turnover. There is also evidence that CatB is implicated in the pathology of chronic inflammatory diseases of airways and joints, and in cancer and pancreatitis. CatB is a 30 kDa bilobal protein. The active site and substrate-binding cleft are located at the interface between the two lobes. Peptide bond cleavage is catalysed by a cysteine residue Cys29 on the left lobe that interacts with a histidine residue His199 on the right lobe. In the specialized environment of the active site, the thiol and imidazole side chains of Cys29 and His199 form an ion pair over the pH range 4.0–8.5. Cleavage of the substrate peptide bond is mediated by nucleophilic attack by S^- from Cys29 on the carbonyl carbon atom, followed by proton donation from His199. CatB plays a dual role as endopeptidase and exopeptidase; in the latter the occluding loop is responsible for this activity. Inhibitors of CatB include endogenous inhibitors such as the cystatin superfamily and low molecular weight natural and synthetic inhibitors, i.e., leupeptin, E-64, CA030. Therefore, search for new inhibitors of CatB, especially selective reversible nonpeptidal inhibitors, should be given increased emphasis.[1–3]

In the previous paper, we reported three biflavones, namely amentoflavone (AMF1), 4‴-methylamentoflav-

Keywords: Cathepsin B; Amentoflavone; FlexX docking; QSAR.
* Corresponding author. Tel.: +86 871 522 3800; fax: +86 871 522 3800; e-mail: nhtan@mail.kib.ac.cn

0968-0896/$ - see front matter © 2005 Elsevier Ltd. All rights reserved.
doi:10.1016/j.bmc.2005.05.071

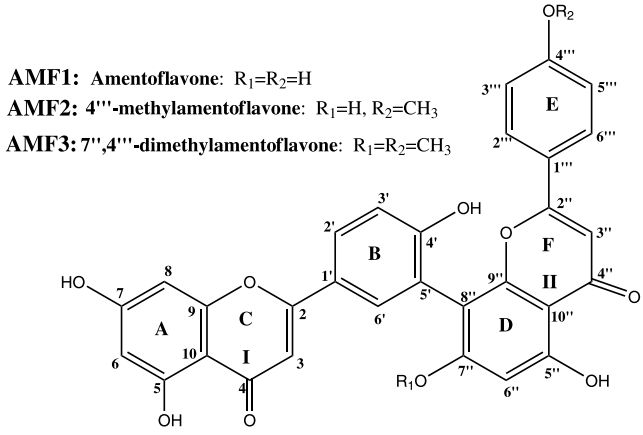

Figure 1. Structures of AMF1, 2, 3.

one (podocarpusflavone A, AMF2) and 7″,4‴-dimethylamentoflavone (4′, 7-dimethylamentoflavone, AMF3) (Fig. 1), as novel natural inhibitors of human CatB, which were isolated from leaves and branches of *Taxodium mucronatum* and showed significant inhibitory activities on CatB with IC_{50} values of 1.75, 1.68 and 0.55 μM, respectively.[4] Amentoflavone is found in a number of plants with medicinal properties, including *Ginkgo biloba* and *Hypericum perforatum* (St. John's Wort), which is a negative modulator GABA at $GABA_A$ $\alpha_1\beta_2\gamma_{2L}$ receptors expressed in *Xenopus laevis* oocytes.[5]

This paper describes our initial efforts towards a structure–activity relationship (SAR) and binding mechanism of AMFs with inhibitory activities on CatB using density functional theory (DFT) method and FlexX program by Sybyl6.9 package on Silicon Graphics R10000 workstation.

2. General modeling and docking strategies

The geometrical structures of AMFs were fully optimized by DFT method at the B3LYP/6-31G* level of theory. Then, the electron properties were obtained by adding keywords pop=full at the B3LYP/6-311G** level of theory.[6–8] These calculations were carried out with the program Gaussian98W.[9]

The protein models were constructed based on the X-ray crystal structure of the 1CSB with the covalently bound inhibitor EXO-EPO-Ile-Pro-OH (CA030) because it has the highest resolution from all available human CatB structures in the Brookhaven Protein Data Bank (2.1 Å).[10,11] The binding pocket of the Cathepsin B was defined with the following amino acid residues: Gln23, Cys29, Gly74, His110, His111, Val176, Leu181, Met196, Gly198, Trp221 and Glu245 with a radius of 6.5 Å around these amino acid residues.

Docking of ligands AMF1, AMF2 and AMF3 to the active sites of the receptor proteins was performed using FlexX (Tripos, St. Louis, MO), which is a fast, flexible docking method using an incremental construction algorithm to place ligands into an active site. Standard parameters of the FlexX program as implemented in Sybyl6.9 were used during docking. Docking produced 30 possible docked conformations for each of the three ligands and the Cscore™ program of SYBYL scored each conformation. Cscore™ is a consensus scoring program that integrates multiple well known and extensively applied scoring functions from the scientific literature, namely, RMSD values,[12] G_score,[13] D_score,[14] ChemScore,[15] PMF_score[16] and FlexX_score.[17] Thus, it can offer multiple approaches for the evaluation of ligand–receptor interactions and the strengths of individual scoring functions combine to produce a consensus that is both more robust and more accurate than any single approach currently in use. Among the 30 conformational solutions of three ligands, the ones with the best FlexX_score (total_score) were chosen as the optimal conformational pose in this study. The ranking first-conformation showed the best binding interactions compared to other solutions.

Ligplot[18] was used to generate hydrogen bonds and hydrophobic interactions between the best-docked conformational pose of the ligand and the amino acid residues in the active site of the protein.

Visual molecular dynamics (VMD) software[19] was used to visualize the binding mode of the docked protein–ligand complexes by generating a connolly type surface for hydrophobic residues of the active sites based on the X-ray structure of 1CSB. The ligand geometry structure was performed on PC and docking on Silicon Graphics R10000 workstations.

3. Results and discussion

3.1. Geometry structure

AMF1, AMF2 and AMF3 possess a similar skeleton except for the difference in 7″ and 4‴ substitutes, but they have the similar geometry structure. Herein, the geometry structure of AMF1 was used to elucidate the characteristics of AMFs structure in this section as one example (Fig. 2). AMF1 is a dimer of apigenin linked at 5′–8″ and makes a dihedral angle of −114.4° (θ_2) between two apigenin units which is a conjugated molecule because most bond lengths of C–C are in the range of 1.34–1.49 Å. All corresponding bond distances and bond angles in two apigenin units (I and II) are in good agreement except for the difference in θ_1 and θ_3. Two benzopyranone moieties (A–C-ring, D–F-ring) are nearly planar, which become rigid for the result of two intramolecular hydrogen bonds O4–H5–O5 (1.69 Å) and O4″–H5″–O5″ (1.68 Å). Two rigid ring systems, i.e., phenyl and benzopyranone moieties, make dihedral angles of 162.2° (θ_1) and 155.4° (θ_3), respectively. It can be seen that θ_1 is not equal to θ_3 as a result of intramolecular π–π interactions between B-ring and E-ring.[20,21] The most interesting structural feature of AMF1 is the rigididity of benzopyranone moiety as well as flexibility between phenyl ring and benzopyranone because the torsional angles θ_1, θ_2 and θ_3 can twist from 0° to 360°.

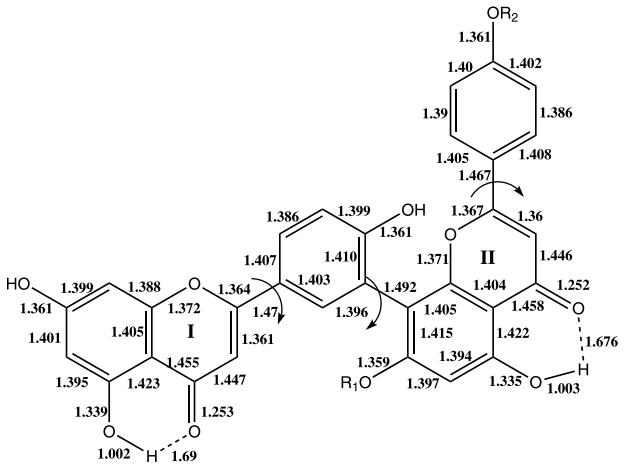

Figure 2. Geometry of AMFs optimized by B3LYP/6-31G* (bond-length in angstroms; $\theta_1 = \theta_{6'\text{-}1'\text{-}2\text{-}1}$; $\theta_2 = \theta_{9''\text{-}8''\text{-}5'\text{-}6'}$; $\theta_3 = \theta_{6'''\text{-}1'''\text{-}2''\text{-}1''}$).

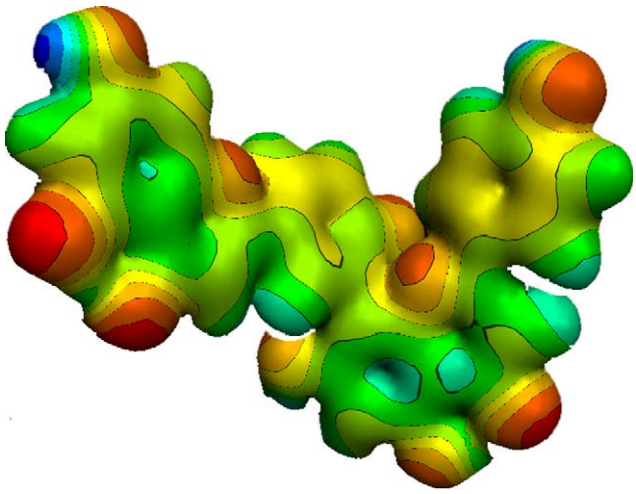

Figure 3. The electrostatic potential for AMF1.

3.2. Atomic charge polarization

Our calculations of the Mulliken charges for AMF1, AMF2 and AMF3 in the gas phase at the B3LYP/6-31G* level are given in Table 1. The results demonstrated that the partial negative charge mainly located at oxygens O1, O4, O5, O7, O4′, O1″, O4″, O5″, O7″ and O4‴, whereas positive ones lay at hydrogen directly bonded to oxygen atom. The O7″ charge (−0.3390) of AMF3 is larger than the charge of O7″ (−0.0845) for AMF2 and the corresponding O7″ atomic charge (−0.0840) of the AMF1. In addition, the atomic charges of corresponding oxygen atom have the similar in the order of AMF3 > AMF2 > AMF1. These results suggested that the methoxyl substitutions at the 7″- and 4‴-positions not only increase the corresponding oxygen atom electrostatic value, but also influence the remote electrostatic charges at the O1, O4, O5, O7, O4′, O1″ and O5″ position.

The electrostatic potentials for AMF1, AMF2 and AMF3 have been calculated and corresponding 3-D structures have been visually analyzed.[22] In Figure 3, we have given the electrostatic potential for the AMF1 ligand. We clearly observed the possibility of strong interaction sites due to the oxygen atoms, indicated by strong negative electrostatic potentials (red) which may participate in electrostatic and/or hydrogen bonds. The hydroxyl hydrogens H7 and H4‴ have a large positive charge indicated by strong positive potentials (blue), which can facilitate interaction with a nearby polar residue from the receptor.

Table 1. HOMO, LUMO energy and most significant oxygen atomic partial charges obtained from a Mulliken population analysis (HLG = $E_{HOMO} - E_{LUMO}$)

Compound	AMF1	AMF2	AMF3
E_{HOMO} (eV)	−6.1218	−6.1076	−6.0948
E_{LUMO} (eV)	−2.2300	−2.1990	−2.1598
HLG (eV)	−3.8918	−3.9087	−3.9351
O7	−0.0986	−0.0988	−0.0989
O5	−0.0907	−0.0909	−0.0912
O4′	−0.1014	−0.1009	−0.1012
O7″	−0.0840	−0.0845	−0.3390
O5″	−0.0794	−0.0800	−0.0786
O4‴	−0.0947	−0.3381	−0.3384

3.3. HOMO and LUMO energy

The orbital energies of both HOMO and LUMO, which are the quantum-chemical descriptors correlated with various biological activities, were calculated for the optimal structures[23] and are reported in Table 1. The AMF3 ligand has a higher HOMO (−6.0948 eV) and lower LUMO (−2.1598 eV) energies than the other two ligands (AMF2, with HOMO = −6.1076 eV and LUMO = −2.1990 eV; AMF1, with HOMO = −6.1218 eV and LUMO = −2.2300 eV). In particular, we noted that the energy gap of HOMO–LUMO (HLG) of AMF3 is smaller (−3.951 eV) than the corresponding HLG values of the other two ligands (AMF2, with HLG = −3.9087 eV and AMF1, with HLG = −3.8918 eV). More specifically, the HLG of AMFs is a negative value which favors the distribution of electron density because HLG is a critical parameter determining the molecular admittance. It can be said that the larger the HLG value, the more stable the molecule and, thus, the harder the rearrangement of its electron density under the presence of an external charge or external electric field.[24] These results also supported that the methoxyl substitutions at the 7″ and 4‴ positions are favorable for inhibitory activity of AMFs.

A well-definite separation was evidenced in the distribution of HOMO and LUMO energies which are located in two distinct parts of the molecule (Fig. 4). It can be seen that the HOMO and LUMO are π-like orbitals.[25] The HOMO energy lay mainly on the A-, B- and C-ring, favoring a strong electrostatic or π–π stack interaction with the residues of the receptor. On the other hand, the LUMO energy mainly located on the D-, E- and F-ring in which the negatively charged polar residues of the receptor are favorable. These results demonstrated that the HOMO and LUMO energy distribution is

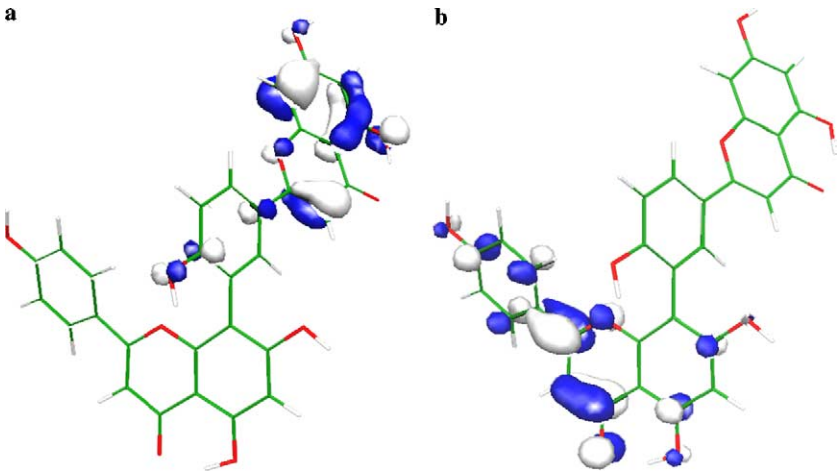

Figure 4. The distribution of HOMO (a) and LUMO (b) energy.

essential for inhibitor activity of AMFs because the most probably involved electron-donor site is the A-ring which shows the highest HOMO energy distribution, while the most important electron-acceptor site is the F-ring which shows the highest LUMO energy distribution.

3.4. Docking AMFs into CatB

AMF1, AMF2 and AMF3 were docked into CatB using FlexX program implanted in Sybyl6.9 package, which created 30 docked conformations for each inhibitor. Docked conformations for each inhibitor were chosen on the basis of the FlexX total energy score, which estimated the binding free energy of a docked inhibitor. The predicted binding free energies of AMF1, AMF2 and AMF3, which were calculated by Cscore^{TM} scoring functions, are listed in Table 2. A correlation was found between the inhibitory activity of AMFs and Cscore^{TM} scoring functions, namely FlexX_score (based on empirical functions), PMF_score (based on statistical ligand–receptor atom–pair interaction potentials), D_score (based on both electrostatic and hydrophobic contributions to the binding energy), G_score (based on hydrogen-bonding interaction) as well as Chem_score (based on a diverse training set of 82 receptor–ligand complexes). It is observed that the produced scoring values for AMF1, AMF2 and AMF3 have shown good correlation with the respective inhibitory activities, i.e., AMF3 has lower scoring values and higher inhibitory activity than those of AMF2 and AMF1. This rather good correlation demonstrated that the binding conformations and binding models of AMFs to CatB are reasonable.

Table 2. Cscore^{TM} scoring values for complexes of the human Cathepsin B receptor with optimal structure of AMFs ligands

Ligand	AMF1	AMF2	AMF3
RMSD (Å)	5.29	5.56	5.52
Total_score	−47.74	−49.06	−52.10
PMF_score	−24.86	−25.34	−25.53
G_score	−83.16	−106.89	−114.74
D_score	−101.06	−103.23	−111.65
Chem_score	−22.18	−22.76	−24.74

Lower scores indicate more favorable binding.

To visualize the binding of three ligands within the active sites, the whole X-ray structure and hydrophobic surface of CatB were superimposed on the best-docked conformations of ligands AMF1, AMF2 and AMF3, respectively. As observed in Figure 5, AMF1, AMF2 and AMF3 were docked in the active site of CatB with a significant different binding mode compared with CA030. Furthermore, Table 2 indicated that the heavy atom root mean square deviation (RMSD) between the docked AMFs and co-crystallized CA030 conformations was 5.29, 5.56 and 5.52 Å, respectively. Those values are larger than the well-known value in theory (RMSD < 1 Å), indicating that we have successfully discovered the most probable binding mode for AMFs. In the case of AMF2 and AMF3, there is not any significant difference in the binding mode because the RMSD values are close to each other ranging from 5.56 to 5.52 Å. By contrast, differences in the binding mode were observed for AMF1 and AMF2 because the RMSD values are 5.29 and 5.56 Å, respectively. As indicated in Figure 5, the 4‴-methoxyl substitution does not favor AMFs binding to CatB due to the fact that AMF1 has a lower RMSD value than those of AMF2 and AMF3. This prediction is in agreement with the experimental results that the residue Glu245 of CatB at the S3 position prefers OH group than CH_3 group.[26] Therefore, any large substitution at the 4‴-position of AMFs may lead to collision with residue Glu245 in the S3 pocket of CatB.

To further validate the binding mode of AMFs, the software Ligplot was employed to study the hydrophobic and hydrogen bond interactions between AMFs and CatB. As depicted in Figure 6, there are hydrophobic interactions between the residue Cys29 and the 3-position at C-ring of AMFs, which is in agreement with the inhibiting mechanism of irreversible inhibitors that

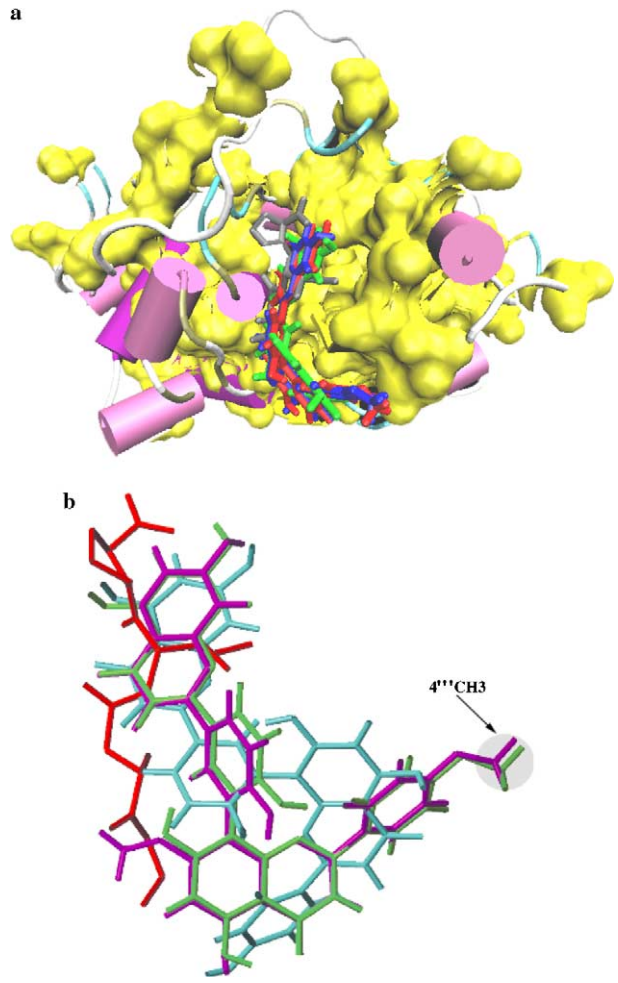

Figure 5. Docking results of the complexes between the AMFs ligands and human CatB. (a) The binding conformations of CA030, AMF1, AMF2 and AMF3 displayed inside the active site of CatB. The inhibitors are displayed in stick model representation with different colors for each compound: Ca030 in gray, AMF1 in green, AMF2 in red and AMF3 in blue. The hydrophobic surface is displayed in a schematic representation in yellow. This figure was prepared using VMD; (b) Superposition of AMF1 (in sky-blue), AMF2 (in green) and AMF3 (in blue) onto known inhibitor CA030 (in red).

residue Cys29 plays a pivotal role in CatB catalyzed mechanism. The hydrogen bonds between each AMF1, AMF2, AMF3 and residue Gln23 with bond lengths of 2.16, 2.40 and 2.39 Å are a good evidence to support the experimental conclusion that residue Gln23 is the S1′ active center of CatB. More attention should be paid to the residue Trp221 because it not only interacts via π–π stacking interaction with the A-ring of AMFs, but also forms a hydrogen bond with the O5 of each AMF1, AMF2, AMF3 with bond lengths of 2.60, 2.69 and 2.70 Å. In the case of AMF1, the C-ring, B-ring, D-ring and F-ring form hydrophobic interactions with the residues His199, Gly73, Gly197 and Gly198, suggesting that more hydrophobic substitutions on those rings should improve AMF1 inhibitory activities. Interestingly, there is one hydrogen bond between O4‴ of AMF1 and residue Glu245 (bond length is 2.44 Å), but not in AMF2 and AMF3, supporting the RMSD conclusion that O4‴ substitution should collide with the residue Glu245. In AMF2 and AMF3, there is one hydrogen bond between O1″ and Gly198 (bond lengths are 3.24 and 3.18 Å), and hydrophobic interactions between F-ring and residues Gly197 and Met195. Surprisingly, AMF2 can form a hydrogen bond with the residue His111 whose bond length is 3.21 Å, supporting the conclusion that CatB has broad active sites. It is observed that B-ring and O7″-CH_3 of AMF3 form hydrophobic interactions with the residues His199, Trp30 and Cys29 because O7″-CH_3 substitution should improve inhibitory activities.

4. Conclusion

In this work, SAR analysis together with FlexX docking was carried out to explore the binding mechanism of AMFs to human CatB, and to provide important information about AMF–CatB interactions, which is essential for the development of selective and reversible biflavone inhibitors of CatB. Through geometry and electron structure analysis of AMFs, it was observed that the CH_3 substitute at 7″ and 4‴ positions could not vary the difference in the geometry structure significantly, but increase the electron density of A-ring, HOMO energy and hydrophobic property. It is proposed that more CH_3 substitutes on the benzyl ring will easily facilitate the electron structure and hydrophobic property, and improve inhibitory activity. Our calculation results supported the experimental observation that the inhibitory activity order is AMF3 > AMF2 > AMF1 which is in agreement with the number of methoxyl substitutions on AMFs.

Both the binding conformations of three biflavones and their binding energies were determined and predicted by molecular docking. The binding energies, estimated by Cscore™ functions, were found to have a good correlation with the experimental inhibitory potencies. Based on the binding conformations from molecular docking, the π–π interaction between A-ring and residue Trp221, two hydrogen bonds (O5 and Trp221; O4 and Gln23), hydrophobic interaction between the C-ring and residue Cys29 and the CH_3 substitutes at 7″ and 4‴ might play a crucial role in the inhibition of AMFs on CatB.

Full geometry optimization of the AMFs ligands and analysis of Mulliken, electrostatic potential, frontier orbitals, energy gap and FlexX can improve our comprehension on the behavior of these potential natural inhibitors and give a reliable model. Our results confirmed that AMFs inhibitors have different binding patterns and interaction modes compared with inhibitors of CA030 analogs that mainly interact with the residues His110, His111 and Cys29 of CatB. In summary, these findings demonstrated that AMFs are new natural reversible inhibitors and could have enormous benefits for the development of new strategies for the rational design and screen of such potent analog inhibitors of CatB.

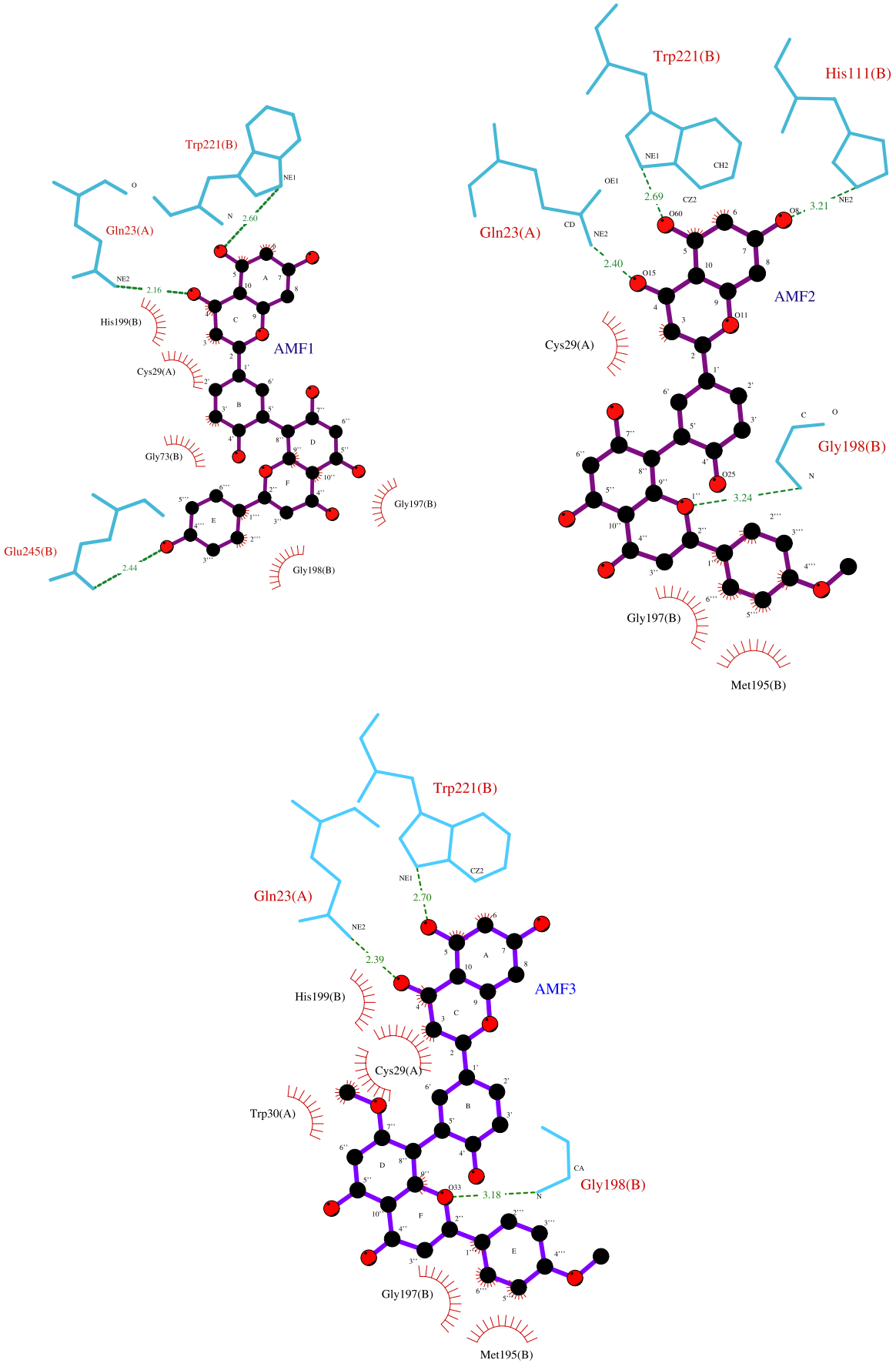

Figure 6. Binding modes of the optimal conformation poses of AMFs ligands with the active sites of CatB receptor. Proposed interaction model of inhibitors AMF1, AMF2 and AMF3 in the active sites of CatB was drawn using the Ligplot program. Broken lines represent hydrogen bonds and spiked residues form van der Waals contacts with the inhibitors.

Acknowledgments

The present work was supported by the Foundation of Chinese Academy Sciences (West Light Program, KSCX1-09-03-1 and KSCX-SW-11) and the 863 Project of China (2001AA234011).

References and notes

1. Mort, J. S.; Buttle, D. J. *Int. J. Biochem. Cell Biol.* **1997**, *29*, 715–720.
2. Zeng, G.-Z.; Tan, N.-H.; Jia, R.-R.; Pan, X.-L. *Acta Bot. Yunnanica* **2005**, *27*, 337–354.
3. Otto, H.-H.; Schirmeister, T. *Chem. Rev.* **1997**, *97*, 133–171.
4. Zhang, Y.-M.; Tan, N.-H.; Huang, H.-Q.; Jia, R.-R.; Zeng, G.-Z.; Ji, C.-J. *Acta Bot. Yunnanica* **2005**, *27*, 107–110.
5. Hanrahan, J. R.; Chebib, M.; Davucheron, N. L. M.; Hall, B. J.; Johnston, G. A. R. *Bioorg. Med. Chem. Lett.* **2003**, *13*, 2281–2284.
6. Benney, G. J.; Peter, M. W. G.; Pople, A. J. *J. Chem. Phys.* **1993**, *98*, 5612–5626.
7. Beck, A. D. *J. Chem. Phys* **1993**, *98*, 1372–1377.
8. Kohn, W.; Beck, A. D.; Parr, R. G. *J. Chem. Phys.* **1996**, *100*, 12974–12980.
9. http://www.gaussian.com.
10. Turk, D.; Podobnik, M.; Popovic, T.; Katunuma, N.; Bode, W.; Huber, R.; Turk, V. *Biochemistry* **1995**, *34*, 4791–4797.
11. Yamamoto, A.; Tomoo, K.; Matsugi, K.-I.; Hara, T.; Yasuko, I.; Murata, M.; Kitamura, K.; Ishida, T. *Biochim. Biophys. Acta* **2002**, *1597*, 244–251.
12. Gohlkea, H.; Hendlicha, M.; Klebe, G. *J. Mol. Biol.* **2000**, *295*, 337–356.
13. Jones, G.; Willett, P.; Glen, R. C.; Leach, A. R.; Taylor, R. *J. Mol. Biol.* **1997**, *267*, 727–748.
14. Kuntz, I. D.; Blaney, J. M.; Oatley, S. J.; Langridge, R.; Ferrin, T. E. *J. Mol. Biol.* **1982**, *161*, 269–288.
15. Eldridge, M. D.; Murray, C. W.; Auton, T. R.; Paolini, G. V.; Mee, R. P. *J. Comput. -Aided Mol. Des.* **1997**, *11*, 425–445.
16. Muegge, I.; Yvonne, C. M. *J. Med. Chem.* **1999**, *42*, 791–804.
17. Rareya, M.; Kramera, B.; Lengauera, T.; Klebeb, G. *J. Mol. Biol.* **1996**, *261*, 470–489.
18. Wallace, A. C.; Laskowski, R. A.; Thornton, J. M. *Prot. Eng.* **1995**, *8*, 127–134.
19. Humphrey, W.; Dalke, A.; Schulten, K. *J. Mol. Graphics* **1996**, *14*, 33–38.
20. Roberto, A.; Pier, L. B.; Gabriella, B.; Paolo, D. R.; Nicoletta, M.; Fiorella, M.; Piero, V. *Il Farmaco* **2003**, *58*, 875–881.
21. Jianga, R.-W.; Yeb, W.-C.; Woob, K.-Y.; Dua, J.; Cheb, C.-T.; Paul, P.-H. B.; Thomas, C. W. K. *J. Mol. Struct.* **2002**, *642*, 77–84.
22. Galeazzia, R.; Marucchinib, C.; Orenaa, M.; Zadra, C. *J. Mol. Struct.* **2003**, *640*, 191–200.
23. Sundaram, A.; Masatoshi, M. *Chem. Res. Toxicol.* **2004**, *17*, 348–356.
24. Robert, G. P.; Ralph, G. P. *J. Am. Chem. Soc.* **1983**, *105*, 7512–7516.
25. Cao, H.; Pan, X.-L.; Li, C.; Zhou, C.; Deng, F.-Y.; Li, T.-H. *Bioorg. Med. Chem. Lett.* **2003**, *13*, 1869–1871.
26. Alpay, T.; Harvey, K.; Sytwu, I.-I.; Vlattas, I.; Regine, B.; Anna, K. K.; Tomoko, H.; Carol, P. H.; Sadiq, H. *J. Biol. Chem.* **1995**, *270*, 18036–18043.